https://doi.org/10.5194/essd-2026-928
Preprint. Discussion started: 26 November 2026
© Author(s) 2026. CC BY 4.0 License.



Open Access Earth System Science Data Discussions

Ocean surface wave advanced parameters from the SWIM instrument on board CFOSAT

Jérôme Lebreton[1], Matthias Averseng[2], Charles Peureux[2], Danièle Hauser[3], Lotfi Aouf[4], Cédric Tourain[5], Annabelle Olivier[2]

[1]CS GROUP, Toulouse, France

[2]Collecte Localisation Satellites (CLS), Ramonville St Agne, France

[3]Université Paris Saclay, CNRS, Sorbonne Université, LATMOS, UVSQ, Guyancourt, France

[4]CNRM-CNRS, UMR-3589, Université Toulouse 3, Météo-France, Toulouse, France

[5]Centre National d'Etudes Spatiales (CNES), Toulouse, France

Corresponding authors: Jerome Lebreton (jerome.lebreton@cs-soprasteria.com) and Danièle Hauser (daniele.hauser@latmos.ipsl.fr)

Abstract. The China France Oceanography Satellite launched in 2018 provides globally and systematically since mid-2019 the directional spectra of ocean waves at a scale of about 70 x 90 km on each side of the satellite-track. These products are quite unique among all oceanographic satellite products and complete very usefully the wave spectra provided by the Synthetic Aperture Radar missions like Sentinel-1 and the significant wave height provided by the altimeter missions. Directional wave spectra contain a lot of information on different scales of waves, which is not straightforward to users to extract the most important wave parameters from such data sets. Here we present a new data set generated in differed-time from the SWIM/CFOSAT operational products, which contains estimates of the Stokes drift (near surface current induced by the wind waves), parameters of the directional wave spectra chosen to characterize more synthetically the shape of the wave spectra and (directional and frequency spread), and indicators proposed in the literature to characterize extreme wave conditions (Benjamin-Feir index, groupness index, cross-sea index). The choice of parameters is discussed, and the definition of each parameter is recalled. A first analysis of the global distribution of these parameters is then presented, and their spatial evolution in a ship accident near the coasts of Australia case study is discussed. With the description of this new data set, we aim to ease the use of SWIM observations for end users and specific marine applications.

https://doi.org/10.5194/essd-2026-928
Preprint. Discussion started: 26 November 2026
© Author(s) 2026. CC BY 4.0 License.



Open Access Earth System Science Data Discussions

1 Introduction

Ocean surface waves are the evident manifestation of the atmospheric forcing by the wind at the ocean surface. Measuring the properties of these wind-generated ocean waves is key for many operational applications and for scientific studies.

Wave forecasting mainly relies on numerical models based on prognostic equations for the evolution of the wave height spectrum (Wamdi group, 1988). Although the wave forecast accuracy has impressively increased in the last 20 or 30 years (Cavaleri et al, 2007; Bidlot, 2017), observations are still required to constrain the numerical solutions of the models through assimilation of observations, and to further improve the model physical parameterizations or to validate them. This is particularly crucial for modeling the evolution of extreme events (severe storms, tropical cyclones).

Because waves affect many processes at the air-sea interface, their observation is also needed to better understand and represent the coupled atmosphere-ocean system. On the atmospheric side, waves impact the atmospheric boundary layer by modulating momentum, heat and gas fluxes (Giordani et al., 2026). On the ocean side, waves play a key role in the turbulent mixing under the surface (Breivik et al., 2014; Law-Chune and Aouf, 2018), induce a near-surface current identified as the Stokes drift, which plays an important role on the ocean mixing in the upper layers (Webb and Fox-Kemper, 2015) and interacts with currents to contribute to Langmuir circulations (Leibovich, 1983; Thorpe, 2004). In the coastal regions, waves contribute to the water level increase during storm events (Melet et al., 2018) and play a major role in sediment transport and coastal erosion. At high latitudes, waves contribute to the processes governing the sea-ice evolution in the marginal ice zone (Rabault et al., 2026; Voermans et al., 2020).

Ocean surface waves are commonly described by their directional elevation density spectrum, which characterizes the distribution of wave energy as a function of wave frequency (or wave number) and of wave propagation direction. In practice, the full information of directional spectra is seldom discussed. Instead, the information is most often reduced to the significant wave height, which characterizes the total energy of waves, and the mean or peak period and direction of the full spectrum or of 2 to 3 partitions. However intrinsically, the wave spectra contain much more information, in particular on directional spread and frequency spread, two parameters which are essential to characterize the non-linear processes governing the wave evolution (Socquet-Juglard et al., 2005) and which can be used to build indexes of extreme wave probability (Janssen and Bidlot, 2009; Mori et al., 2011). In addition, the Stokes drift can be estimated from the wave spectrum and depends on the spectral shape. In numerical wave models, the obtained spectral shape is a result of the parameterization and numerical approximations (Alves and Banner, 2003; Zieger et al., 2015; Forristall and Greenwood, 1998; Gagnaire-Renou et al. 2010; Rogers and Van Vledder, 2013; Rogers and Wang, 2007), but its validation is rare because of the lack of reference data. So, although the numerical mode outputs are commonly validated in terms of significant wave heights, their validation in terms of dominant frequency and direction is less frequent, and the validation of

https://doi.org/10.5194/essd-2026-928
Preprint. Discussion started: 26 November 2026
© Author(s) 2026. CC BY 4.0 License.


spectral shape is extremely rare. This is probably due to the lack of references, as wave data from in situ measurements are mostly available in coastal regions and often reduced to mean wave parameters.

Launched in 2018, the China-France Oceanography Satellite (CFOSAT) provides at the global scale the wave height spectrum at a scale of about 70 km x 90 km on each side of the nadir satellite track (Hauser et al., 2021). This data set is unique as it is the only one providing systematically and at the global scale the full directional spectra of ocean waves. In contrast, altimeters only provide the significant wave height (sometimes the mean period but with strong assumptions), whereas side looking SAR measurements provide spectra of the ocean long swell part only, and with potential distortions due to the so-called velocity bunching effect (Alpers and Brüning, 1986).

The principle of measurement for CFOSAT is based on the analysis of the radar backscatter measured by the SWIM (Surface Waves instrument and Monitoring), which is a real-aperture radar carried by CFOSAT (Hauser et al., 2017, 2021) and pointing at near-nadir incidences (0 to 10° from nadir). Since the CFOSAT launch, many studies have been devoted to the validation of this data set (Hauser et al., 2021; Wang et al, 2022; Ying et al., 2022; Canto et al., 2026) and continuous improvements have been brought to the data processing (Tourain et al., 2023). One outcome of these studies is that the best configuration for the SWIM measurement is when the 10° beam incidence is used to estimate the wave spectra. Several scientific analyses have shown the usefulness of these spectral observations (Le Merle et al., 2022; Meucci et al., 2023; Li et al., 2024; Pouplin et al., 2024; Zhao et al., 2024; Badulin et al., 2025; Bedossa et al., 2026).

In France, the SWIM data are processed in near real-time by the national space agency CNES to provide Level-2 products which contain wave height spectra from the different SWIM beams (6° to 10°). These products, called L2, are made available in near-real time to users through the data portal AVISO (see how to access in Sect. 6). In addition to this near real-time products, a delayed time processing is applied to propose two products: the so-called L2P products, which are still directional spectra but only from the 10° incidence observations and with less ancillary variables, and the so-called L2P_derived products, which contain parameters derived from the full-directional spectra (from the 10° beam only) to characterize the spectral shape (in both frequency and direction), several associated indexes related to the probability of extreme waves, as well as the Stokes drift velocity.

This paper describes the new L2P_derived demonstration dataset, that has been generated in 2026 by reprocessing all the SWIM 10° beam data from April 2019 to June 2026. The paper is organized as follows. In Section 2, we present the main characteristics of the directional wave spectra provided by the SWIM instrument that is used to provide this new data set. In Section 3, we present the definitions and expressions used for the new parameters provided and illustrate these parameters in some examples. In section 4, we present a first analysis of the global distribution of these parameters as well as their spatial evolution during a ship accident off the Australian coasts. Finally, we conclude in Section 5.

https://doi.org/10.5194/essd-2026-928
Preprint. Discussion started: 26 November 2026
© Author(s) 2026. CC BY 4.0 License.



2 SWIM wave spectra and basic wave parameters

From the SWIM observations, various wave products for users are processed and made available to users. They are described below. All are accessible from the CNES AVISO+ data portal through https://www.aviso.altimetry.fr/en/missions/current-missions/cfosat/access-to-data.html after registration to the service.

In near real-time (i.e. less than 3 hours after observations sensing) the so-called "L2 products" are made available by the CNES ground segment. These L2 products contain the significant wave height Hs estimated from the nadir beam, and the directional wave spectra $S(k,\theta)$ expressed as wave slope spectra and estimated from the 6°, 8°, and 10° SWIM beam observations. Each wave spectrum is estimated with a sampling of 15° in direction without resolving the 180° ambiguity in direction (provided over 12 directional bins) and since version 7 of the processing for 40 wavelengths unequally spread from 22 to 1112 m (instead of 32 wavenumbers up to 500 m wavelength in version 5 of the processing). Directional spectra are built by combining observations from successive overlapping azimuthal scans, so that each spectrum is representative of an area (called "wave box") sizing approximately 70 km along-track by 90 km across-track. Wave boxes are defined all along the satellite track, with boxes on each side of the satellite track. Associated with these wave spectra, the L2 products also provide the mean parameters of the wave spectra and of up to 3 wave partitions (significant wave height, dominant wave direction, dominant wavelength). The current wave spectrum processing includes a normalization of the total wave energy by using the significant wave height value provided by the nearest nadir beam measurement (using the so-called MTF3 Modulation Transfer Function). More details are provided in Hauser et al, 2021. Note that since the early results shown in this paper, several improvements have been brought in the processing. In particular, the speckle model has been refined, parasitic peaks are filtered out, and the range of wavelength provided in the product has been extended. An example of a directional spectrum provided in the L2 products is shown in Fig. 1. This example illustrates a case of mixed sea with wind waves (dominant wavelength of about 70 m aligned NE-SW) superposed with two long swells (230 and 320 m in wavelength).

https://doi.org/10.5194/essd-2026-928
Preprint. Discussion started: 26 November 2026
© Author(s) 2026. CC BY 4.0 License.



Open Access Earth System Science Data Discussions

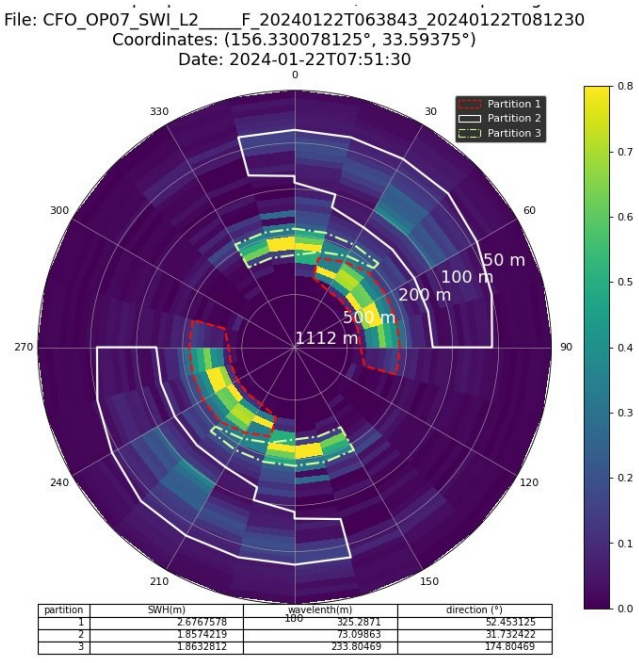


Figure 1: Example of wave slope spectrum and associated wave parameters provided in the L2 product. It corresponds to observations at 33.6 N, 156.3 E, on January 24th, at 7:51 UTC. The spectral energy of the directional wave slope spectrum is represented by the color code. The direction is plotted from 0 to 360°, with the vertical axis towards the geographic North and the 180° ambiguity represented in this plot. The wavelength scale is shown with concentric circles from 50 m (outer circle) to about 1100 m (most inner circle). Three wave partitions are identified (red solid line, white solid line, white dashed line,), ranked by energy level. The associated main parameters are indicated in the table below the polar plot.

The second available product is the L2P_box product, which is directly derived from the L2 but contains a more restricted list of variables: they contain only the wave slope spectra from the 10° SWIM beam observations. The rationale of this product is to select the most essential variables obtained with the most reliable data sets for users. Indeed, it was previously shown in several studies that the 10° beam observations provide the best performance when compared to model or observations (Hauser et al., 2021; Xu et al., 2022). So, only the wave spectra and associated parameters from the 10° beam observations are kept in the L2P_box product. Furthermore, to be consistent with other types of directional wave spectra data sets, the spectra has been symmetrized to provide a spectrum over [0-360°]. Note that for these products, the processing used for the wave partitioning method differs by some details from that used in L2 processing (smoothing ahead of partitioning, merging of low energy partitions), but the wave partitioning still relies on the watershed method. This L2P product is available in delayed time (a few days after acquisition) on https://www.aviso.altimetry.fr/en/data/products/wind/wave-products/wave-wind-cfosat-products.html.

https://doi.org/10.5194/essd-2026-928
Preprint. Discussion started: 26 November 2026
© Author(s) 2026. CC BY 4.0 License.



Finally, the third product is the L2P_derived (or L2PDER) which provides variables that can be estimated from the wave spectra. This is the purpose of the present paper to describe the content of these L2P_derived products and show some illustrations of these parameters. This product is available through the AVISO+ data portal (CNES) at https://doi.org/10.24400/527896/a01-2024.005 (Collecte Localisation Satellites, 2025).

3 New wave parameters

3.1 Definitions

3.1.1 Stokes drift

The Stokes drift is the Lagrangian mean flow resulting from the depth-dependent decay of ocean surface wave orbital motions, slower at depth and faster near the surface, which produces a net drift in the direction of wave propagation. It is a key quantity that affects the dynamics, thermodynamics, and transport of matter in the upper ocean. While it is mostly significant at the ocean surface, it can remain significant down to a few tens of meters below. All wavelengths contribute to the Stokes drift, but the shorter waves contribute the most to the surface current. The Stokes drift estimation in the L2PDER products relies on a physically consistent framework combining direct integration of the observed directional wave spectra and parametric reconstruction of unresolved spectral components. The Stokes drift vector $U_s(z)$ at depth z is computed from the directional wave height spectrum $E(k,\theta)$ under the deep-water approximation as (Kenyon, 1969):

$$U_s(z) = 2\sqrt{g}\int_0^{\infty} k^{\frac{3}{2}} e^{2kz}\left[\int_0^{2\pi} E(k,\theta)\boldsymbol{u}\, k d\theta\right] dk \quad (1)$$

where k is the wavenumber, $u=[cos\theta,sin\theta]^T$ the unit vector in the direction of the wave propagation, and g the gravitational acceleration.

In practice, the Stokes drift is decomposed into two contributions:

$$\mathrm{U}_S(z) = \mathrm{U}_S^L(z) + \mathrm{U}_S^S(z) \quad (2)$$

where $U_s^L(z)$ represents the contribution from long waves directly resolved by the SWIM instrument, and $U_s^s(z)$ corresponds to the contribution from shorter waves not captured within the instrumental spectral range.

The separation between resolved and unresolved scales is defined by the maximum wavenumber k_{max} accessible in the SWIM spectra. This value is determined by the upper limit of the SWIM spectral grid, which depends on the instrument

https://doi.org/10.5194/essd-2026-928
Preprint. Discussion started: 26 November 2026
© Author(s) 2026. CC BY 4.0 License.



Open Access Earth System Science Data Discussions

configuration and processing version. In the current L2 processing, SWIM directional spectra typically extend up to k_{max} ~ 0.28 rad m^{-1}, corresponding to wavelengths of about 22–30 m. As a result, only wave components with wavelengths longer than this threshold are directly observed, while shorter waves can be parameterized.

The long-wave contribution (referred to as the "raw" Stokes drift) is therefore computed by discrete integration of the SWIM spectra over the resolved wavenumber range [0, k_{max}], after conversion from slope spectra *S(k,θ)* to elevation spectra using Eq. (3):

$$E(k,\theta) = \frac{S(k,\theta)}{k^2} \tag{3}$$

and after resolving the intrinsic 180° directional ambiguity by assuming that the waves propagate at ±90 deg from the wind (using collocated wind direction from the ECMWF atmospheric model as wind direction reference)

The contribution of unresolved short waves is estimated using a parametric approach based on theoretical wind-wave spectra. In particular, the high-wavenumber tail of the omnidirectional spectrum is assumed to follow a Phillips-type behavior (Phillips, 1958):

$$E(k) = \alpha_p k^{-3} \tag{4}$$

where the Phillips constant α_p is estimated from the highest resolved wavenumber bins of the SWIM spectrum. The directional distribution is further parameterized following established formulations for wind-driven waves (Elfouhaily et al., 1997), enabling reconstruction of the directional properties of unresolved waves. Under these assumptions, the short-wave contribution is computed from k_{max} to infinity as:

$$U_S^S(z) = 2\sqrt{g}\int_{k_{max}}^{\infty} k^{\frac{3}{2}} E(k)\, m_1(k)\, e^{2kz}\, dk \tag{5}$$

where $m_1(k)$ represents the first directional moment of the spectrum.

This combined approach ensures that the reconstructed Stokes drift profile is consistent with the observed SWIM spectra over the resolved range while accounting for the significant contribution of high-wavenumber waves beyond k_{max}, which dominate the near-surface Stokes drift but are not directly observed by the instrument (Breivik et al., 2014).

https://doi.org/10.5194/essd-2026-928
Preprint. Discussion started: 26 November 2026
© Author(s) 2026. CC BY 4.0 License.

Open Access Earth System Science Data Discussions

The Stokes drift is provided in the L2PDER dataset at two representative depths: at the ocean surface (z = 0 m) and at a subsurface level (z = −15 m), allowing users to capture both the near-surface signal strongly influenced by short waves and a deeper signal less sensitive to high-frequency contributions (Breivik et al., 2014; Webb and Fox-Kemper, 2015).

For each depth, two complementary estimates are distributed in the L2PDER product. The "raw" Stokes drift corresponds to the contribution from waves directly resolved by the SWIM spectra, i.e. the integration up to k_{max}. The "full" Stokes drift includes an additional contribution from unresolved short waves, estimated through the parametric spectral reconstruction described above, by extending the integration beyond k_{max} using theoretical spectral formulations (Phillips, 1958; Elfouhaily et al., 1997).

This dual representation allows users to distinguish between the directly observed component of the wave-induced transport and a more complete estimate that accounts for the important contribution of short wind-generated waves, especially in the near-surface layer.

In Figure 2, we compare the values obtained from the SWIM spectra over 26 days of observation (2 SWIM cycles from early January 2024 to early February 2024), to those estimated from collocated spectra provided by the French version of the WAM wave model (referred as ECW AMIFS-38R2), run without SWIM data assimilation, and with a parameterization taken from the ST4 version of the WW3 model (Ardhuin et al., 2010). For estimations from WAM, Eq. (1) was used with an upper integral limit corresponding to the highest frequency of the model (~2π/5 m). Figure The agreement between SWIM-derived and WAM-derived Stokes drift estimates is the best when considering the Stokes drift at 15 m depth (Fig. 2b and Fig. 2d) with a bias of 0.03 m, a rmse of 0.16 m/s and a scatter index (SI) of 19%. At this depth, results are almost similar with (Fig. 2d) or without (Fig. 2b) extrapolation of the SWIM wave spectrum. This is because with the exponential term in Eq. (1), the contribution of short waves decays rapidly with depth. In contrast when the Stokes drift is estimated at the surface from SWIM without accounting for contributions of waves shorter than the smallest detected waves (Fig. 2a), the agreement with WAM decreases significantly (bias: -2.74 m/s, rmse; 3.46 m/s, SI: 36 %). Because the Stokes drift is strongly weighted toward the high-frequency (short-wavelength) part of the wave spectrum, the unresolved tail of the SWIM spectrum leads to an underestimation of the surface Stokes drift (Fig. 2a). Adding a high-wavenumber spectral completion compensates for this missing energy and significantly improves the agreement with WAM-derived estimates at the surface (Fig. 2c).

https://doi.org/10.5194/essd-2026-928
Preprint. Discussion started: 26 November 2026
© Author(s) 2026. CC BY 4.0 License.

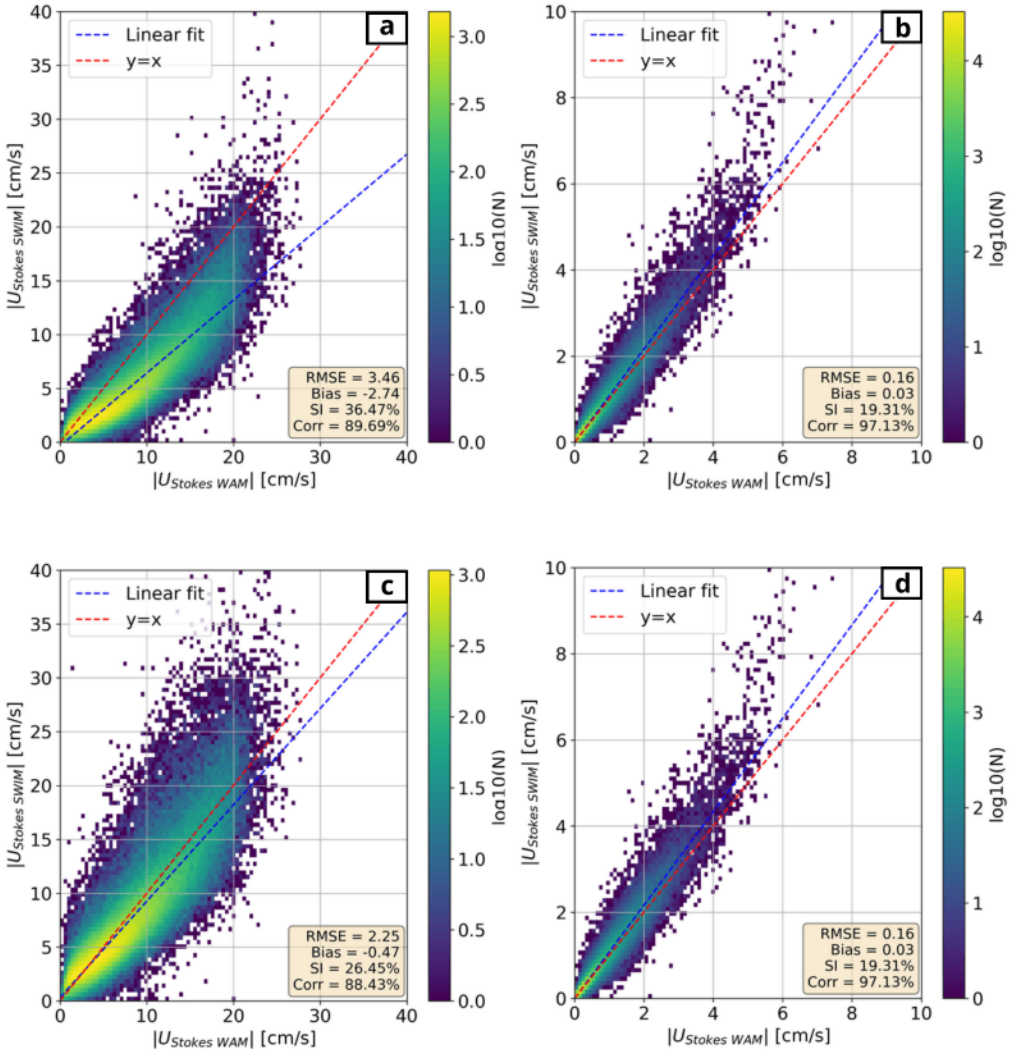
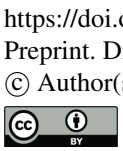


Figure 2: Scatterplots of the Stokes drift velocity estimated from SWIM observations against values estimated from colocalized WAM model spectra. The left column (a and c) corresponds to the surface (0 m) and the right column (b and d) to a depth of 15 m. The top row (a and b) compares Stokes drift contributions derived directly from the original SWIM spectra with those obtained from colocalized WAM spectra. The bottom row (c and d) compares Stokes drift velocities derived from SWIM spectra completed with a high-frequency spectral tail to the corresponding WAM estimates. Colors indicate the logarithm of the number of collocated observations. The blue dashed line represents the linear regression, while the red dashed line denotes the 1:1 relationship.

https://doi.org/10.5194/essd-2026-928
Preprint. Discussion started: 26 November 2026
© Author(s) 2026. CC BY 4.0 License.



Open Access Earth System Science Data Discussions

Figure 3 (a, c and d) compares maps of the monthly mean Stokes drift values at the surface from SWIM and WAM spectra. The SWIM values are those obtained with spectra completed at high wavenumbers. These maps reveal a strong spatial consistency between both estimations, with maximum differences of about 5 cm/s in the Southern Ocean and in regions of mid-latitude storms (Fig. 3d). There is also a strong spatial consistency of the Stokes drift and the ECMWF wind field (Fig. 3b). The largest Stokes drift magnitudes (about 20 cm/s) are observed in regions of persistent strong winds, such as the Southern Ocean, the North Atlantic and North Pacific. This behaviour is expected since according to Eq. (1), and due to the shape of the wave spectrum with wavenumber, the Stokes drift magnitude is increased in the presence of young short waves (wind seas), which remain strongly coupled to the local wind forcing in this region. Consequently, a clear geospatial correspondence is observed between the magnitude of the Stokes drift contribution, its vector components, and the wind field. In some tropical regions however, this correspondence is less evident (tropical South Pacific for example). This is explained in this case, by the combination of swell and low wind conditions. In these regions, the relative contributions of long waves on the Stokes drift are increased. Overall, the similarity in both amplitude and direction highlights the coherence of the large-scale patterns captured by the SWIM-derived and WAM-derived Stokes drift fields.

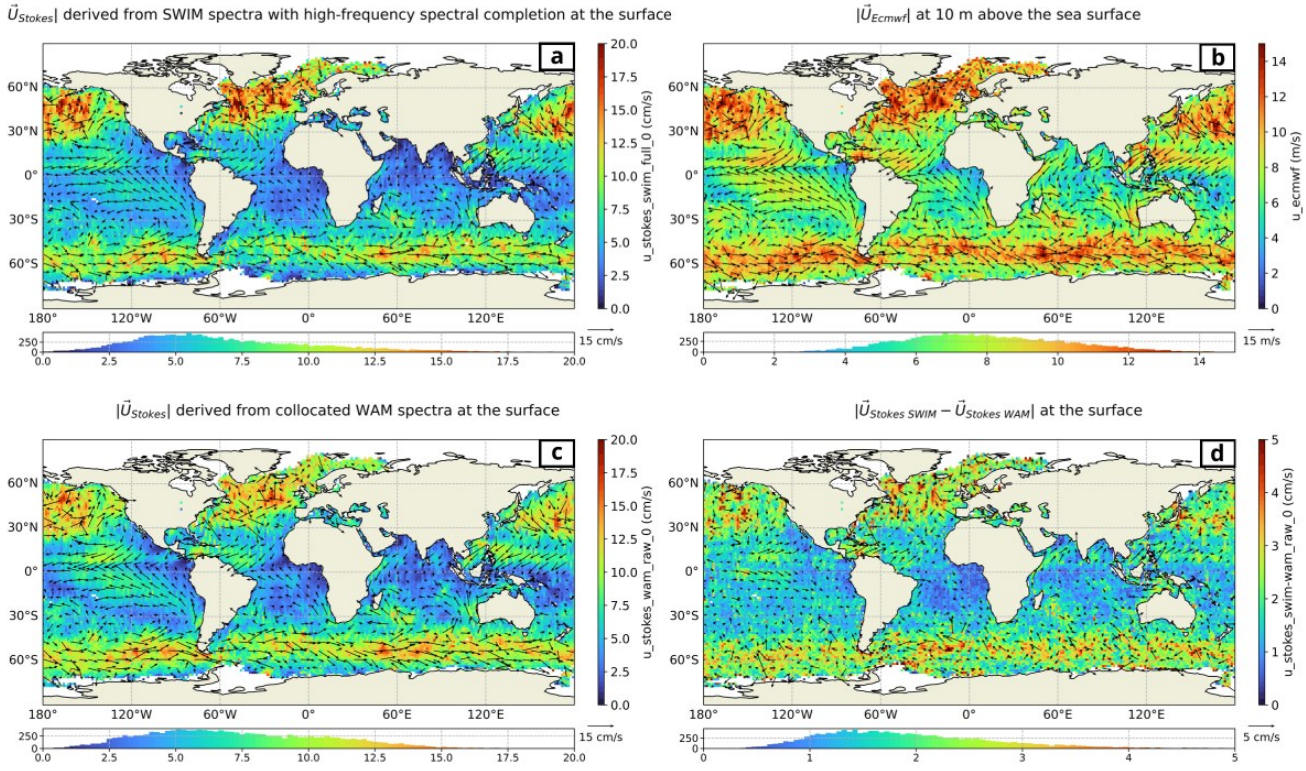


Figure 3: Monthly mean global distribution of the surface Stokes drift magnitude and direction derived from SWIM spectra completed at high wavenumbers (a), collocated WAM spectra (c), and the absolute difference between both estimates (d), after

https://doi.org/10.5194/essd-2026-928
Preprint. Discussion started: 26 November 2026
© Author(s) 2026. CC BY 4.0 License.



spatial averaging over 2° × 2° grid cells. The corresponding ECMWF 10 m wind field, averaged over the same grid, is shown in (b). Colours indicate the field magnitude (cm/s for the Stokes drift and m/s for the wind speed), while arrows represent the field direction. The analysis is based on observations and model outputs averaged over the study period.

3.1.2 Wave spectral shape parameters

The set of parameters considered in this section is designed to characterize both omni-directional and directional (2D) wave spectra. These parameters are commonly adopted in literature by wave modeling communities to describe key aspects of sea state dynamics. They are used to assess the likelihood of extreme wave events, including rogue waves, through indicators such as the Benjamin–Feir index, as well as the probability of extreme conditions associated with crossing seas (e.g., cross-sea index, cross-trough correlation). Additionally, they provide insight into the influence of wave grouping on significant wave height variability. To ensure consistency with standard definitions, most of these parameters require the transformation of wave spectra from the wavenumber domain, as provided in SWIM products, into the frequency domain. This conversion is performed under the assumption of deep-water conditions, which allows the application of the linear dispersion relation.

For all parameters, except the so-called peakedness 2D parameter, the following dispersion relation for deep water waves is first used to transform the wave height spectrum expressed in wavenumber $E(k,\theta)$ into a wave height spectrum expressed in frequency $E(f,\theta)$. The frequency f is calculated as follows:

$$f = \frac{\sqrt{gk}}{2\pi} \tag{6}$$

with g the gravitational acceleration and k the wavenumber. Also, to ensure the conservation of the total spectral energy, the following equivalence applies:

$$E(f,\theta)df\,d\theta = E(k,\theta)k\,dk\,d\theta \tag{7}$$

Thus, the spectral density expressed in frequency is related to the spectral density expressed in wavenumber by:

$$E(f,\theta) = k\,E(k,\theta)\frac{8\pi^2 f}{g} \tag{8}$$

De Carlo et al. (2023) introduced a two-dimensional peakedness parameter to characterize the degree of energy concentration in both wavenumber and directional space. They showed that this parameter provides a robust metric to

https://doi.org/10.5194/essd-2026-928
Preprint. Discussion started: 26 November 2026
© Author(s) 2026. CC BY 4.0 License.



investigate wave group effects and the spatial variability of significant wave height. The 2D peakedness is defined in Eq. 8 with $E(k,\theta)$ the directional wave spectrum expressed as a function of wavenumber k and direction θ:

$$Q_{kk} = \left(\frac{\iint E^2(k,\theta) k \, dk \, d\theta}{(\iint E(k,\theta) k \, dk \, d\theta)^2} \right)^{\frac{1}{2}} \quad (9)$$

The directional properties of the wave field can be quantified through the mean directional spread, which describes the angular dispersion of wave energy. This parameter is widely used to characterize the degree of directional spreading and to distinguish between unidirectional and multi-directional sea states. Following Kuik et al. (1988), the directional distribution is described using the first-order Fourier coefficients of the directional spectrum in Eq. (10) and Eq. (11):

$$a_1 = \iint cos\theta \, E(f,\theta) df d\theta \quad (10)$$

$$b_1 = \iint sin\theta \, E(f,\theta) df d\theta \quad (11)$$

Then, the mean directional spread is calculated as follows:

$$\sigma_\theta = \sqrt{2\left(1 - \sqrt{\frac{(a_1^2 + b_1^2)}{m_0^2}}\right)} \quad (12)$$

The mean directional spread quantifies the angular width of the wave energy distribution, with small values of σ_θ indicating a narrow directional distribution, typical of well-organized wave systems and large values reflecting a broad spreading of energy, characteristic of complex or crossing sea states.

Cross-sea conditions, characterized by the coexistence of wave systems propagating in significantly different directions, are known to enhance the probability of extreme and potentially hazardous sea states. In this context, Météo-France, within the framework of the MaxWave project (Rosenthal et al, 2008), proposed a cross-sea index (Eq. (13) designed as an operational warning indicator for such conditions. This index is based on the combination of the directional spreading of wave energy and the significant wave height H_s, thereby capturing both the geometric complexity of the sea state and its energetic intensity.

https://doi.org/10.5194/essd-2026-928
Preprint. Discussion started: 26 November 2026
© Author(s) 2026. CC BY 4.0 License.



Open Access Earth System Science Data Discussions

$$CSI = \frac{H_s}{a} \cdot \exp(-10(\sigma_\theta - b)^2) \quad (13)$$

With $a = 2$ and $b = 1$

From the omnidirectional wave height spectrum expressed in the frequency domain *E(f)*, it is possible to derive the Goda parameter (Goda, 2010) described in Eq. (14). This parameter provides a measure of the omni-directional spectral shape and is commonly used to characterize the narrowness or broadness of the wave energy distribution in frequency space. It is also sometimes referred as the peakedness parameter (Häfner et al. (2021).

$$Q_p = \frac{2 \int E^2(f) f df}{\left(\int E(f)\, df\right)^2} \quad (14)$$

This parameter can be interpreted as an indicator of spectral broadness in the frequency domain with high values of Q_p corresponding to narrow-banded spectra with a strong concentration of energy around the peak frequency, and low values indicating broader spectra with energy distributed over a wider range of frequencies.

Here, we consider the frequency bandwidth σ_{Qf} expressed as a function of Q_p such that narrow spectra (i.e., strongly peaked) correspond to small frequency spreads, while broader spectra are associated with larger values of σ_{Qf}:

$$\sigma_{Qf} = \frac{1}{\sqrt{\pi} \cdot Q_p} \quad (15)$$

Another frequently used parameter to characterize the spectral width is the narrowness parameter defined by Longuet-Higgings (1983) from the moments of the one-dimensional frequency spectrum *E(f)*:

$$m_n = \int f^n E(f) df \quad (16)$$

The narrowness parameter is then expressed as:

$$\sigma_{Narrf} = \sqrt{\frac{m_0 m_2}{{m_1}^2} - 1} \quad (17)$$

https://doi.org/10.5194/essd-2026-928
Preprint. Discussion started: 26 November 2026
© Author(s) 2026. CC BY 4.0 License.



It is an alternative parameter to σ_{Qf} to quantify the spectral bandwidth, with small values corresponding to narrow-banded spectra, where energy is highly concentrated around the dominant frequency, and larger values indicating broader spectra with energy distributed over a wider frequency range.

The crest–trough correlation r has been proposed as a relevant indicator of extreme wave conditions, as it reflects the degree of asymmetry between wave crests and troughs and the underlying structure of the wave field. Häfner et al (2021) and Gemmrich and Cicon (2022) highlighted its usefulness for identifying sea states prone to extreme wave occurrence. This parameter is defined as the autocorrelation of the sea surface elevation evaluated at half the dominant wave period. Following Tayfun and Fedele (2007), the crest–trough correlation noted r can be expressed as:

$$r = \frac{1}{m_0}\sqrt{\rho^2 + \lambda^2} \tag{18}$$

$$where\ \rho = \int E(f)\cos\left(2\pi f\frac{T}{2}\right)df\ ,\ and\ \lambda = \int E(f)\sin\left(2\pi f\frac{T}{2}\right)df$$

$$and\ T = \frac{m_0}{m_1}$$

This formulation expressed in Eq. (18) measures the correlation between a wave crest and the trough occurring half a period later. High values (close to 1) correspond to a high probability of extreme waves.

The generation of rogue waves is commonly associated with the Benjamin–Feir instability, a nonlinear mechanism that is enhanced in spectrally narrow and weakly directional sea states. In this context, Janssen and Bidlot (2009) demonstrated that the ratio between wave steepness and spectral bandwidth plays a key role in controlling the likelihood of extreme wave occurrence due to non-linear four wave interactions. This ratio in Eq. (19), known as the Benjamin–Feir Index (BFI) is defined as:

$$BFI = \frac{\varepsilon}{\sigma}\sqrt{2} \tag{19}$$

where ε denotes the characteristic wave steepness and σ the spectral bandwidth.

The characteristic steepness is expressed as:

$$\varepsilon = k_p\sqrt{m_0} \tag{20}$$

where k_p is the peak wavenumber (estimated as described in the following), and m_0 is the zeroth-order spectral moment.

https://doi.org/10.5194/essd-2026-928
Preprint. Discussion started: 26 November 2026
© Author(s) 2026. CC BY 4.0 License.



The spectral bandwidth σ is derived from the Goda peakedness parameter introduced previously in Eq. (15), ensuring consistency in the description of the spectral shape. To account for directional effects, Mori et al. (2011) proposed an extended formulation of the BFI, which incorporates directional spreading:

$$BFI_{2D} = \frac{BFI}{\sqrt{1+\alpha R}}, \; with \; R = \frac{\sigma_\theta^2}{2\sigma_{Qf}^2} \tag{21}$$

where σ_θ is the mean directional spread (in radians), and σ_{Qf} frequency bandwidth. The coefficient α, determined from numerical simulations, and taken as α = 7.10, following the evaluation of Mori et al. (2011). This parameterization was obtained from a theoretical and numerical study of quasi-resonant four-wave interactions (modulation instability).

This extended formulation highlights the stabilizing effect of directional spreading: narrow-banded and weakly directional sea states (low σ_{Qf}, low σ_θ) lead to high BFI_{2D} values and increased likelihood of extreme waves (increase of the excess kurtosis in the wave height distribution, see Mori et al., 2011). Broader or less directional spectra reduce the BFI_{2D}, thereby limiting the development of modulational instability. The Benjamin–Feir index, is therefore a central parameter for assessing the potential for extreme wave formation due to four wave nonlinear interactions. According to Mori et al. (2011), it may however be not sufficient to fully characterize extreme waves generated by wave/current interactions or in crossing sea-state conditions. It is therefore complementary to other indexes mentioned here above (cross-sea index, cross-trough correlation).

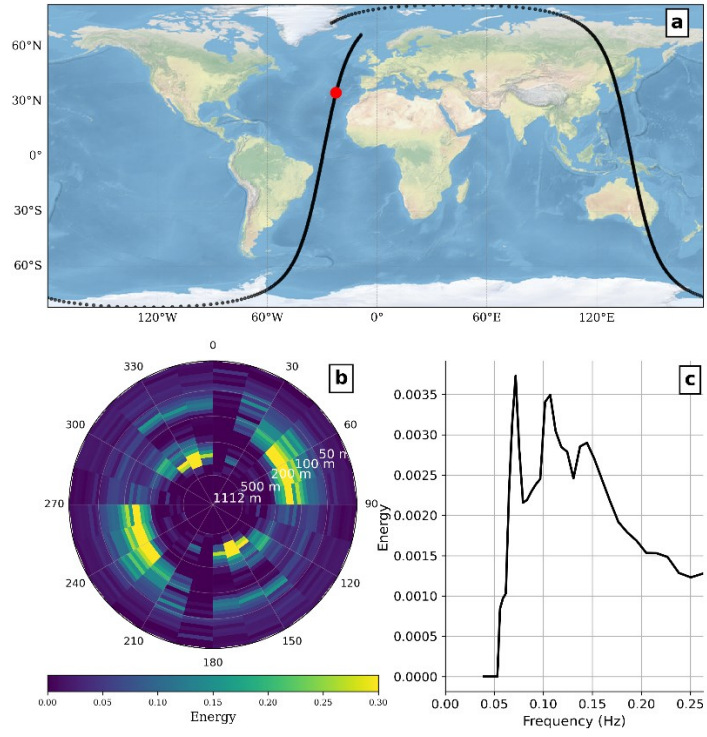
To minimize the influence of spurious or parasitic peaks at low wavenumbers occasionally observed in wave height spectra, a robust approach is adopted to estimate the spectral peak frequency. Such an artefact can bias the identification of the dominant wave component and, consequently, affect the computation of derived parameters. To address this issue, a weighted-mean estimator is employed (Eq. (21)), following Young (1995) and subsequently adopted by Serio et al. (2005) and Häfner et al. (2021). The peak frequency f_p is thus defined as:

$$f_p = \frac{\int E^4(f) f df}{\int E^4(f) df} \tag{22}$$

3.2 Examples

To illustrate these parameters, we show here two spectra (Fig. 4 and Fig. 5) with different sea state conditions and the set of corresponding spectral shape parameters. The first case in Fig. 4 (30° N, subtropical Atlantic) exhibits a multimodal frequency spectrum, with three closely spaced peaks at 0.07, 0.10 and 0.15 Hz of comparable amplitudes, and a broad directional distribution (angular spread of 43.5°), organized into two diffuse components.

https://doi.org/10.5194/essd-2026-928
Preprint. Discussion started: 26 November 2026
© Author(s) 2026. CC BY 4.0 License.



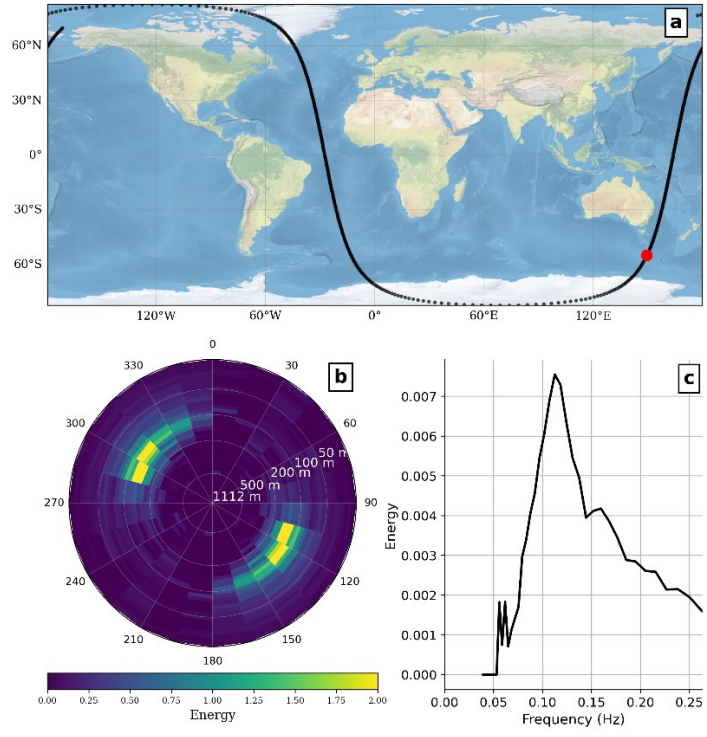
d

Parameter	Value
Goda parameter	1.85
Peakedness from Goda	0.30
Narrowness	0.34
Peakedness 2D	21.43
BFI 1D	0.10
BFI 2D	0.02
Crest-Trough Correlation	0.59
Angular spread	43.47
Cross sea index	0.86
Hs	3.08

Figure 4: Example of wave spectrum and associated parameters on 28/01/2024 at the location marked by the red point in panel (a). Directional wave slope spectrum in panel (b) and (c) omnidirectional wave height spectrum plotted as a function of frequency.

The second case (55°–60° S, Southern Ocean) shows, by contrast, a narrower unimodal spectrum, dominated by a single, distinct peak at 0.11 Hz, and marked directional focus (angular spread of 28.3°), with one distinct energy lobe characteristic of a single wind sea system.

https://doi.org/10.5194/essd-2026-928
Preprint. Discussion started: 26 November 2026
© Author(s) 2026. CC BY 4.0 License.



d

Parameter	Value
Goda parameter	3.28
Peakedness from Goda	0.17
Narrowness	0.28
Peakedness 2D	20.00
BFI 1D	0.41
BFI 2D	0.08
Crest-Trough Correlation	0.74
Angular spread	28.27
Cross sea index	0.20
Hs	5.36

Figure 5: Example of wave spectrum and associated parameters on 28/01/2024 at the location marked by the red point in panel (a). Directional wave slope spectrum in panel (b) and (c) omnidirectional wave height spectrum plotted as a function of frequency.

This contrast in wave characteristics is quantified by multiple parameters. For instance, the cross-sea index, which is significantly higher in the subtropical case (0.86 versus 0.20), confirms the coexistence of several wave systems in this case, as opposed to the dominance of a single system in the Southern Ocean case. This is corroborated by all the spectral shape parameters: the Southern Ocean case exhibits a spectrum that is both narrower and sharper (Goda = 3.28, narrowness = 0.28) than the subtropical case (Goda = 1.85, narrowness = 0.34), with a significant wave height nearly twice as high (Hs = 5.36 m versus 3.08 m), reflecting the influence of a significantly more intense system. The spectral width both in terms of wavenumber and direction observed in the Southern Ocean case is accompanied by a systematic increase in indicators of non-linearity. The *BFI*, either estimated in 1D (0.41 versus 0.10) or in 2D (0.08 versus 0.02), as well as the crest-trough correlation (0.74 versus 0.59), are all higher in this case. These BIF_{2D} values reflect the change in the Benjamin-Feir modulational instability mechanism, according to which a combined narrowing of the frequency and directional bands of the spectrum favors the development of extremely high waves, whereas a broader, multimodal sea where energy where non-linear effects tend to average out. These observations suggest that, beyond the significant wave height alone which is a conventional metric but insufficient for characterizing the danger posed by sea states, other spectral parameters such as those

https://doi.org/10.5194/essd-2026-928
Preprint. Discussion started: 26 November 2026
© Author(s) 2026. CC BY 4.0 License.



mentioned above, provide a relevant indicator of the potential for non-linearity and, by extension, of the risk of extreme wave formation.

4 A first analysis of the spectral shape parameters

4.1 Relationships between the various parameters

A statistical analysis was carried out from one CFOSAT orbital cycle (13 days) in January 2024 to examine the distribution of values and the relationships between the various parameters. The results are illustrated in Fig. 6 with scatter plots between pairs of parameters and histograms of values for each parameter. As expected from their formulation, the *BFI* and BFI_{2D} indexes are strongly correlated (ρ = 0.92), but their respective sensitivities to spectral shape parameters differ. The one-dimensional *BFI*, which depends on the frequency spread of the spectrum, is more strongly correlated with the spectral width of σ_{Qf} (ρ = -0.62) than with the directional spread of σ_θ (ρ = -0.31). In contrast, the BFI_{2D}, which explicitly contains the *R* ratio between directional and frequency spreads, shows an increase in dependence with σ_θ (ρ = -0.57) at the expense of its dependence on σ_{Qf} (ρ = -0.46).

The crest-trough correlation *r* follows the more closely the variations of σ_{Qf} (ρ = −0.81). This correlation decreases slightly when *BFI* is considered and more significantly when BFI_{2D} is considered (ρ = 0.77 with *BFI*, ρ = 0.67 with BFI_{2D}) confirming that the coherence between successive peaks and troughs is governed primarily by the frequency sharpness of the spectrum rather than by its steepness and angular dispersion. This is consistent with the results presented by Gemmrich and Cicon (2022).

The angular spread σ_θ is strongly correlated with the cross-sea index (ρ = 0.84); this is expected as the *CSI* incorporates the angular spread in its formula in Eq. (13).

The *CSI*, by contrast, is only weakly correlated with the *BFI* type indices (ρ = 0.04 with *BFI*, ρ = −0.24 with BFI_{2D}) as well as with σ_{Qf} (ρ = 0.14) and *r* (ρ = −0.11). This decoupling confirms that the *CSI* captures a distinct dimension of wave, focusing on the angular spread of the spectrum rather than the effect of frequency narrowing, unlike the *BFI* and *r*, which remain primarily governed by the frequency width.

Regarding the significant wave height *Hs*, it shows moderate-to-strong correlations with both *BFI* indices (ρ = 0.70 with *BFI*, ρ = 0.73 with BFI_{2D}) as well as with *r* (ρ = 0.61), and negative correlations with the spectral widths σ_{Qf} (ρ = −0.48) and σ_θ (ρ = −0.46). This trend reflects the fact that the most energetic seas are associated with narrower spectra, both in frequency and direction, thereby favoring higher *BFI* and *r* values.

https://doi.org/10.5194/essd-2026-928
Preprint. Discussion started: 26 November 2026
© Author(s) 2026. CC BY 4.0 License.



Open Access Earth System Science Data Discussions

The histograms of each of these parameters indicate that while some of them have a near Gaussian behavior (σ_{Qf}, σ_θ), the others show a very skewed distribution (*BFI*, BFI_{2D}, *r*, *CSI*). These latter are therefore better suited to identify extreme values.

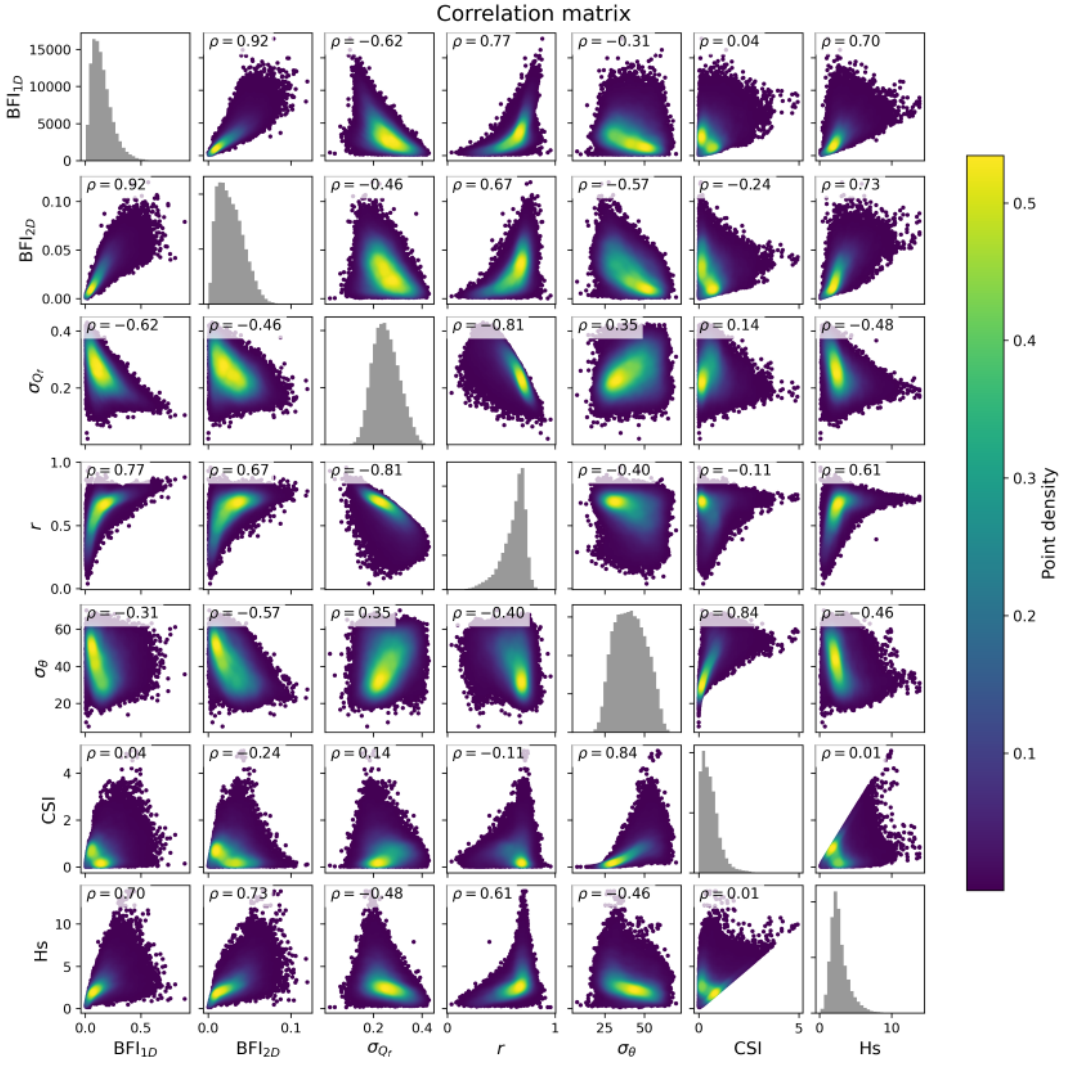


Figure 6: Correlation matrix between shape parameters on 1 cycle from 14/11/2024 to 28/11/2024

https://doi.org/10.5194/essd-2026-928
Preprint. Discussion started: 26 November 2026
© Author(s) 2026. CC BY 4.0 License.

Open Access Earth System Science Data Discussions

4.2 Seasonal Geographical Distribution of Wave Parameters

The geographical distributions of the Cross-Sea Index (*CSI*), Benjamin Feir Index (*BFI*) and crest-trough correlation (*r*) were analysed (Fig. 7, Fig. 8 and Fig. 9) for two contrasted seasons of year 2025: winter (January to March) and summer (June to August). For each parameter, maps derived from SWIM observations are presented in the left column (panels (a) and (c)), while the corresponding WAM model estimates are shown in the right column (panels (b) and (d)). This comparison allows the assessment of the capability of SWIM observations to reproduce the spatial patterns and seasonal variability represented by the WAM model, as well as the identification of regions where significant discrepancies occur.

The comparison of *CSI* values in Fig. 7 reveals significant differences, both in magnitude and in their spatial distribution. Overall, the model values are smaller compared to the SWIM values, and the maximum values evidenced in the model results in the Southern Ocean during both seasons are only partially evidenced in the SWIM data. But in other regions local maxima are Observed for both SWIM and WAM (North Atlantic in both seasons, Indian ocean in summer). These differences may be primarily linked to differences in the directional spread of the spectra, as differences in significant wave height are, in principle, less significant, except perhaps for the most energetic sea states. The SWIM data show that the highest *CSI* values are mainly associated with regions where swell and non-aligned wind-driven waves coexist, particularly in the intertropical regions throughout the year and in the proximity of mid-latitude storms in winter, especially in the North Atlantic and the North Pacific. This distribution suggests a link between high *CSI* values and the co-existence of wave systems exhibiting distinct directional characteristics.

https://doi.org/10.5194/essd-2026-928
Preprint. Discussion started: 26 November 2026
© Author(s) 2026. CC BY 4.0 License.

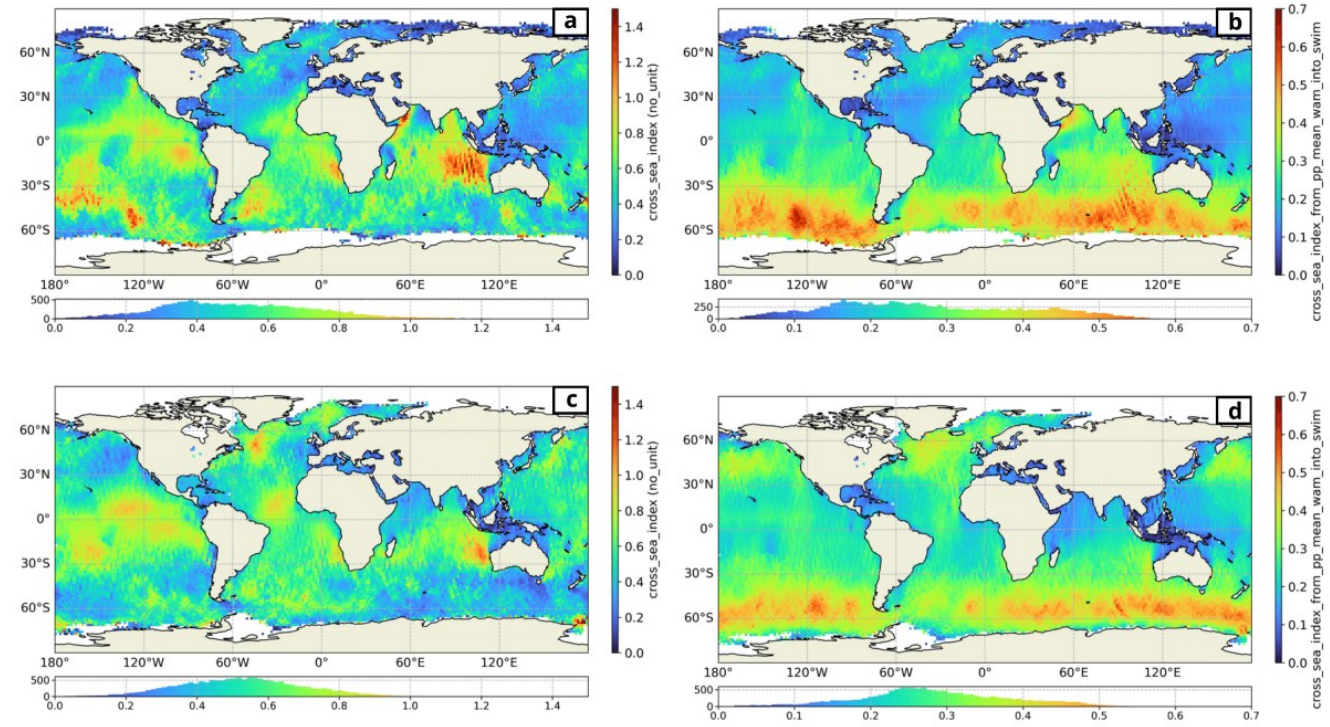


Figure 7: Cross-sea index averaged over 2° x 2° grid cells from SWIM observations (a and c) and collocated WAM model outputs (b and d) during the summer period (June-September 2025, panel a and b) and winter period (March-May 2025, panel c and d).

The differences between SWIM and WAM are less pronounced for the *BFI* in Fig. 8 than for the *CSI*, but differences appear in the geographical distribution of high values. In enclosed seas, SWIM tends to underestimate the *BFI* compared with WAM. This difference may be linked to difficulties in estimating the spectral peak wave number and/or the spectral width parameter, particularly in conditions of young, underdeveloped seas with low *Hs* values. Conversely, in the Southern Ocean throughout the year, and in the proximity of mid-latitude storms in winter, the *BFI* values obtained using SWIM are generally higher than those from WAM. MFWAM is known to underestimate Hs values in the Southern Ocean when no assimilation is used as here (Aouf et al, 2021). So, these differences result from differences in the estimation of k_p and/or σ_{Qf}.

https://doi.org/10.5194/essd-2026-928
Preprint. Discussion started: 26 November 2026
© Author(s) 2026. CC BY 4.0 License.

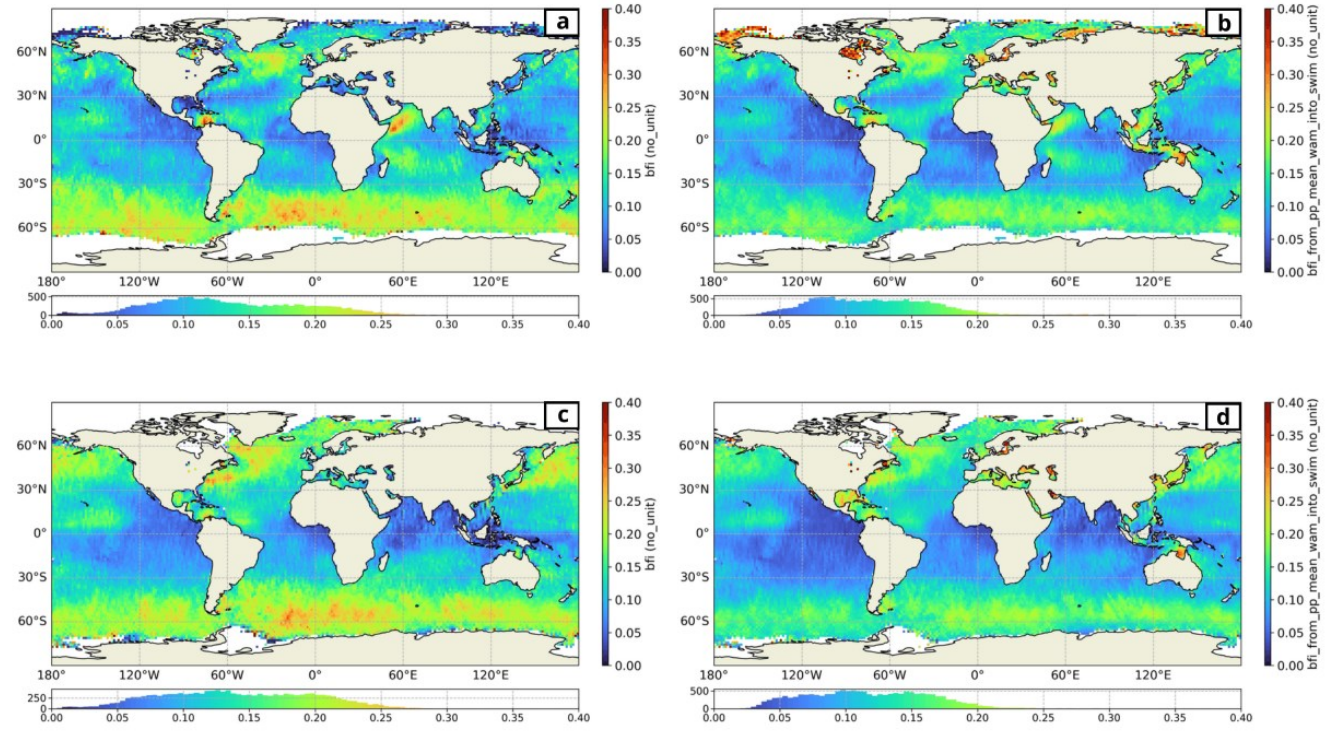


Figure 8: Benjamin Feir Index (BFI) averaged over 2° x 2° grid cells from SWIM observations (left column) and WAM model outputs collocated with SWIM observations (right column) during the summer period (June-September 2025, top row) and winter period (March-May 2025, bottom row).

The crest-trough correlation in Fig. 9 shows a spatial distribution like that of *BFI*, despite the different calculation methods. This similarity is corroborated by a high statistical correlation between the two indices (r = 0.77) discussed in Sect. 4.1. However, it remains to be determined, particularly in the light of Gemmrich and Cicon's (2022) work, to what extent they characterise similar aspects of wave non-linearity and phenomena associated with extreme waves. As with the *BFI*, SWIM tends to significantly underestimate this index in enclosed seas, potentially due to measurement limitations in conditions of young, underdeveloped waves. Conversely, the values obtained using SWIM are generally higher than those from WAM in the Southern Ocean. The origin of these differences remains to be clarified through an analysis of the spectral characteristics and their influence on the index.

https://doi.org/10.5194/essd-2026-928
Preprint. Discussion started: 26 November 2026
© Author(s) 2026. CC BY 4.0 License.

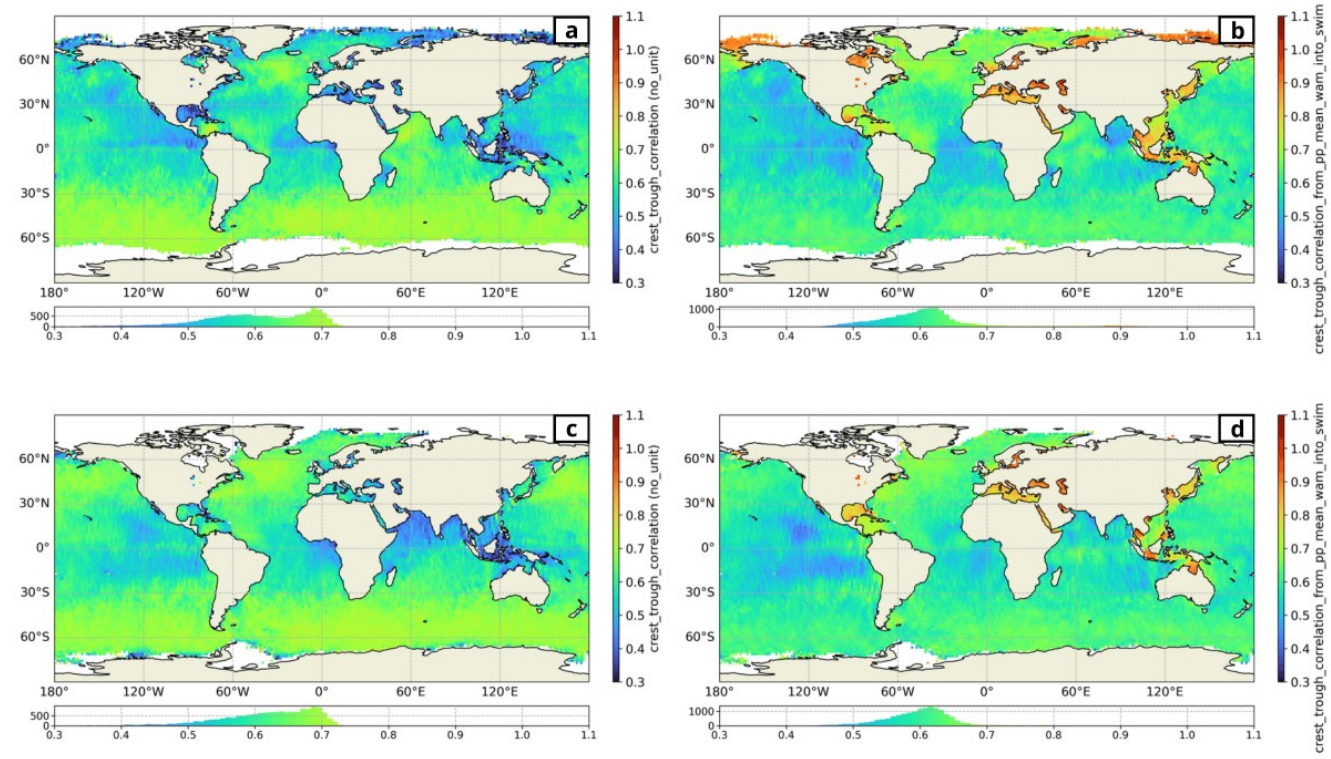


Figure 9: Crest trough correlation averaged over 2° x 2° grid cells from SWIM observations (a and c) and collocated WAM model outputs (b and d) during the summer period (June-September 2025, a and b) and winter period (March-May 2025, c and d).

4.3 A case study

To assess the ability of SWIM observations to characterize dangerous sea state conditions, we consider the case of the container ship APL England on the 24th of May 2020, which suffered a significant loss of cargo off the coast of Sydney. During this incident, 50 containers were lost at sea and a further 79 were damaged because of severe rolling motion in adverse weather conditions. Investigations attributed this incident to a combination of structural and environmental factors, including advanced corrosion of the lashing devices, inadequate maintenance of these devices, and rough sea conditions which exacerbated the loads exerted on the cargo. Here below we analyze SWIM observations acquired few hours after the event.

A local analysis of the 2D and 1D spectra was carried out to illustrate the regimes in the accident zone and outside it. The wave spectrum observed around 40° S (panel d in Fig. 10), shows a relatively diffuse energy distribution, dominated by a wind-driven sea associated with a wavelength of approximately 150 m. This condition corresponds to a weakly structured

https://doi.org/10.5194/essd-2026-928
Preprint. Discussion started: 26 November 2026
© Author(s) 2026. CC BY 4.0 License.

and moderately energetic sea, characterized by a significant wave height of approximately 4.5 m. However, as we approach the accident site, around 35° S, the spectral structure shifts towards a significantly more organized and bimodal pattern. Two distinct energy maxima appear, associated with two swell systems with wavelengths of around 250 m. One of these systems is aligned with the direction of the local wind, whilst the other is offset by approximately 45 to 50°, reflecting the coexistence of two superimposed wave systems. This configuration is typical of a crossing-seas condition. In this case, two wave trains of almost the same wavelength are observed. This spatial transition occurs in the South-North branch of a surface current eddy clearly identified by the streamlines in Fig. 10a, and is associated with an increase in significant wave height from 5 m to 7 m.

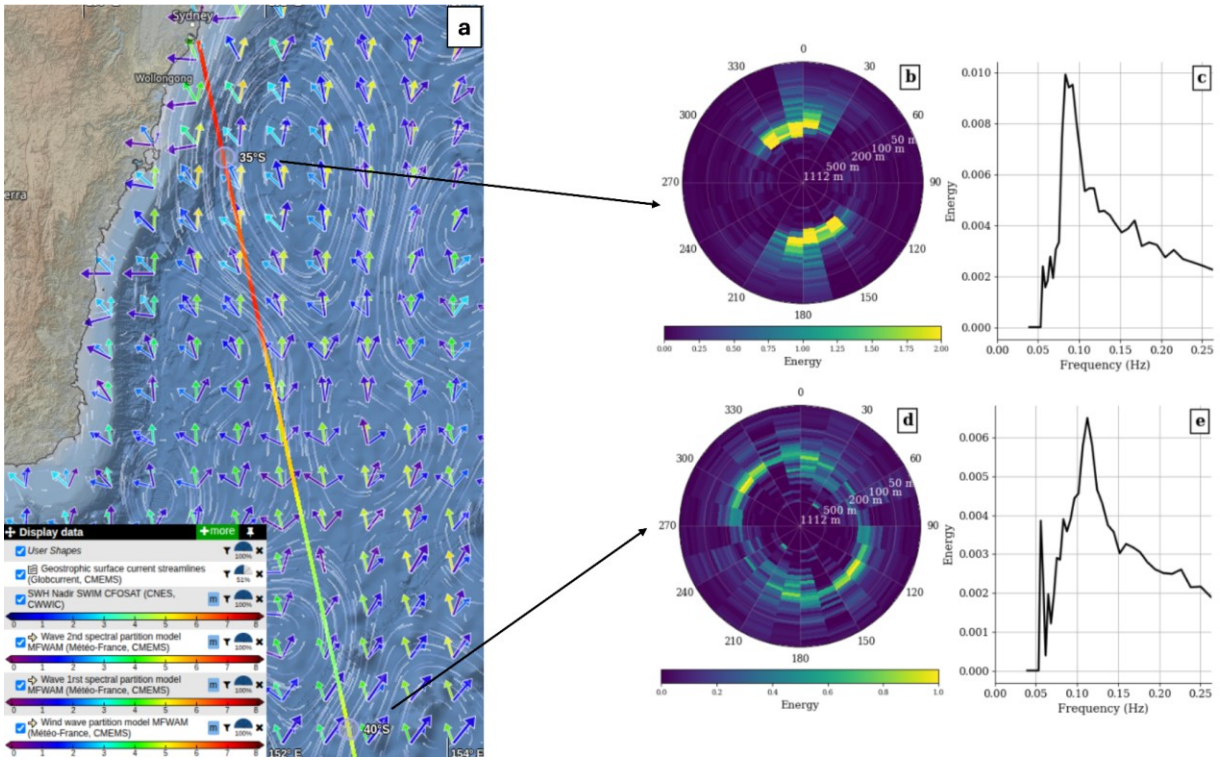
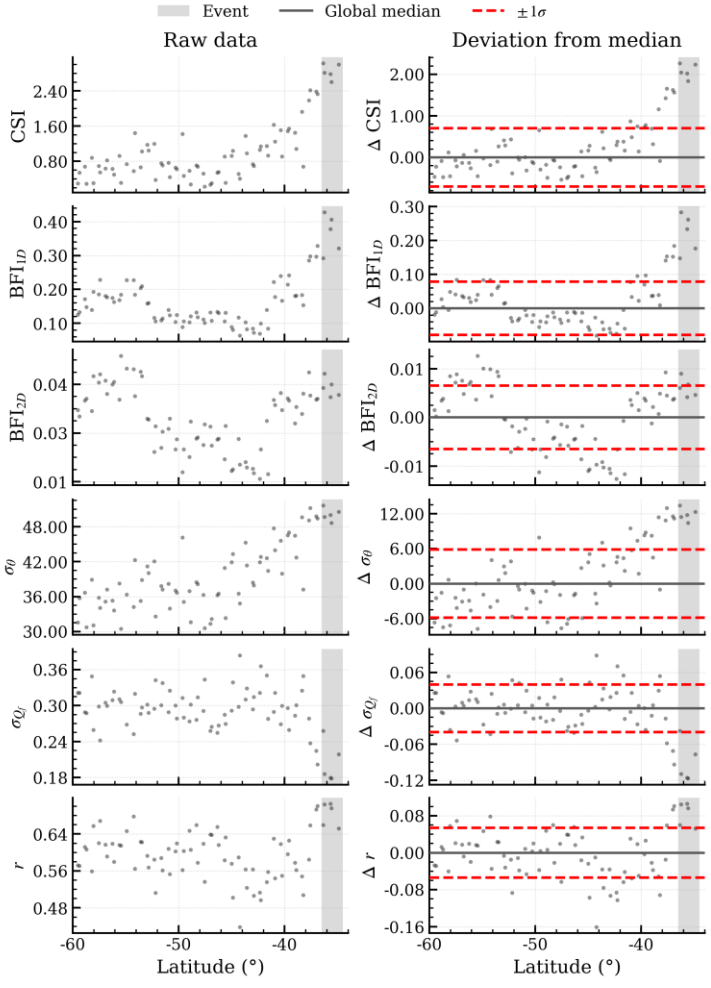


Figure 10: (a) Hs values along the CFOSAT track (color) with current streamlines (light white lines) from the Copernicus Multi Observation Thematic Center (MOB TAC) overlayed; vectors represent the first two swell components and the wind sea component from the MFWAM model (direction and period from the arrow direction and length, significant wave height from the color) (b and c) 2D spectra and 1D spectra at 35° S; (d and e): 2D spectra and 1D spectra at 40° S.

The variation of wave parameters along the CFOSAT track is shown in Fig. 11 to illustrate the changes as the vessel approaches the Australian coast and the accident site. When considering the deviation from the average of the observations, a marked gradient is evident in the proximity of the study area (shown in grey), which is particularly pronounced for the

https://doi.org/10.5194/essd-2026-928
Preprint. Discussion started: 26 November 2026
© Author(s) 2026. CC BY 4.0 License.

spectral width σ_{Qf}, the Cross Sea Index (*CSI*) and the one-dimensional Benjamin–Feir Index. These three parameters show a consistent trend suggesting a transition towards a more narrow-banded, steeper sea state, which could indicate an increase in non-linear wave-wave interactions. However, when combined with the directional spread σ_θ in BFI_{2D}, this leads to BFI_{2D} values remaining within the +- 1 std. This may indicate that the extreme waves encountered during this event are not due to the four wave non-linear interactions described by the BFI_{2D} parameter. In contrast, the crest-trough correlation shows maximum value at the event location. The *CSI* and the *r* coefficient are not specifically related to four wave non-linear interactions (Gemmrich and Cicon (2022) but reflect other non-linear mechanisms that are not considered in the theory associated with *BFI* definitions (Mori et al., 2011), in particular those due to wave/current interactions. So, in the case illustrated here, it seems that *CSI* and *r* are better suited to characterize the extreme conditions encountered during the ship accident.



https://doi.org/10.5194/essd-2026-928
Preprint. Discussion started: 26 November 2026
© Author(s) 2026. CC BY 4.0 License.



Figure 11: Left panel: variation along the CFOSAT track (shown in Fig. 10) of the spectral shape parameters from SWIM observations (from top to bottom: *CSI*, *BFI*, BFI_{2D}, σ_θ, σ_{Qf}). Right panel: relative deviations from the mean value of the same parameters. The red dashed lines indicate the +- 1 std. The grey contours indicate the area of the ship accident.

5 Discussions and conclusions

We have presented a new dataset, generated in differed time from operational observations by the SWIM instrument on board the CFOSAT satellite, which enables a more detailed characterization of sea states on a global scale. In addition to the standard parameters like the significant wave height, wavelength and spectral direction, this dataset provides a set of complementary parameters describing the Stokes drift and the shape of the spectrum (frequency and angular dispersion, non-linearity indices -*BFI* and crest-trough correlation- cross-sea index).

Concerning the Stokes drift, we have shown that the estimate at a depth of 15 m is very consistent with the model values even without extrapolating the wave spectra beyond the maximum frequency sampled by SWIM. At the surface, the agreement is still reasonable provided that the observed wave spectrum is extrapolated in the high frequency range. The assumptions made on the wave propagation direction (to remove the 180° ambiguity) may however slightly bias the results in some regions (Zou et al, 2026). Using ancillary information to remove the 180° ambiguity can improve the results (Zou et al, 2026).

Statistical analysis between the shape parameters highlights the correlations and complementarities between these various indicators, showing that each captures a distinct aspect of spectral features. Moreover, the comparison between SWIM and MFWAM shows that SWIM generally reproduces the main spatial structures despite differences in amplitude, particularly for the CSI. The differences observed, particularly in the Southern Ocean, may also reflect the limitations of MFWAM, which tends to underestimate the significant wave height without assimilation. Conversely, SWIM has certain limitations in enclosed seas and under conditions of low sea state. These results highlight SWIM's potential to characterize wave non-linearity and complement the model's estimates.

The APL England case study illustrated the operational value of these new parameters: the observed transition from a diffuse sea state, dominated by wind-driven waves, to a bimodal cross-sea configuration in the neighbourhood of the incident site, associated with a significant increase in wave height, suggests that spectral geometry is a relevant indicator of the risk of adverse navigational conditions, complementing wave height alone. These new data thus open new perspectives for studying the relationship between spectral shape and sea states in dangerous seas, for both research and operational applications dedicated to safety of ships navigation.

https://doi.org/10.5194/essd-2026-928
Preprint. Discussion started: 26 November 2026
© Author(s) 2026. CC BY 4.0 License.



However, these parameters have certain limitations that should be highlighted. Under low-energy sea conditions (low *Hs*), the signal-to-noise ratio of the spectrum deteriorates, and the impact of spurious peaks becomes more pronounced, which may bias the estimation of spectral shape parameters. However, with the current ongoing studies on the SWIM data processing, we expect better filtering of these low frequency spurious peaks, and thus better estimates of some of the spectral shape parameters. New releases of the L2P_derived products will be made when this is operational.

Also, the angular resolution of the SWIM instrument, which is intrinsically limited by the measurement geometry, restricts the precision with which certain directional parameters, notably angular dispersion σ_θ and, by extension, the indices dependent on it (BFI_{2D}, *CSI*) can be estimated, particularly for wave systems that are close in direction.

The L2P_DERIVED dataset available on the AVISO website covers the entire lifespan of the CFOSAT mission. Thus, it uses as input incremental versions of the L2 products, (currently OP06 and OP07 versions). But we have verified that the differences in the parameters remain generally negligible between these versions. They occur mainly in low-energy wave conditions, characterized by low values of significant wave height (Hs). In the future, the wave spectral products will still be improved thanks to the processing evolution at the L2 level, in particular on-going work to better avoid the wave height spectra spurious peaks at low frequencies. The L2P_DERIVED products will then benefit from these improvements.

6 Data availability

SWIM L2P-derived data sets can be downloaded from the AVISO+ data server using the following link https://www.aviso.altimetry.fr/en/data/products/windwave-products/level-2p-derived-products-from-swim-instrument-of-cfosat.html, after registration as AVISO+ user (https://www.aviso.altimetry.fr/en/data/data-access/registration-form.html). The geographic coverage is global. At the time of publishing this paper, the data set covers the period from April 2019 to June 2026 (1 file per orbit, up to 19-20 files per day).

The dataset Digital Object Identifier (DOI) is https://doi.org/10.24400/527896/a01-2024.005 (Collecte Localisation Satellites, 2025) and is distributed under the Creative Commons Attribution 4.0 International (CC-BY 4.0). The following acknowledgement should appear in publications using this data set: "This SWIM Level-2P Derived product was produced by CLS in the frame of the FRench Oceanographic Ground Segment (FROGS) of the CFOSAT Mission and distributed by AVISO+ with the support of CNES."

Author contributions

JL, MA, CP developed the codes and provided the figures. LA proposed the test case for illustration.

https://doi.org/10.5194/essd-2026-928
Preprint. Discussion started: 26 November 2026
© Author(s) 2026. CC BY 4.0 License.



JL, MA, DH prepared the manuscript with contributions from all co-authors.

Financial support

This study has been funded by the French space agency CNES.

590 **References**

Alves J.H.G.L., and M.L. Banner: Performance of a saturation-based dissipation-rate source term in modeling the fetch-limited evolution of wind waves, J. Phys. Oceanogr., 33, p 1274-1298, 2003

Ardhuin, F., Rogers, E., Babanin, A. V., Filipot, J.-F., Magne, R., Roland, A., et al., Semiempirical dissipation source functions for ocean waves: Part I: Definition, calibration, and validation. Journal of Physical Oceanography, 40(9), 1917–1941, https://doi.org/10.1175/2010JPO4324.1, 2010

Badulin S.I., A. G. Kostianoy, S. A. Lebedev, A. P. Popov: The Caspian Sea as a full-scale experimental facility supported by altimetry measurements of wind-driven waves, Dynamics of Atmospheres and Oceans, 110, 101554 , 2025

Bedossa E., Aouf L.E., A. Dalphinet, D. Hauser, H. Giordani, F. Collard: Long term assimilation of directional wave data from CFOSAT in the wave prediction model MFWAM, Earth and Space Science, 13, e2025EA004743, 2026

600 Bidlot, J-R.: Twenty-one years of wave forecast verification, ECMWF Newsletter Number 150 – Winter 2016/17, doi: 10.21957/t4znuhb842, 2017

Breivik, O. J., Janssen P.A.E.M, Bidlot J-R.: Approximate Stokes Drift Profiles in Deep Water. J. Phys. Oceanogr., 2433-2445, 2014

Canto, M., Khan, S., Young, I. *et al.*: Multiplatform calibration and validation of CFOSAT ocean surface waves. Ocean Dynamics 76, 56, https://doi.org/10.1007/s10236-026-01797-5, 2026

Cavaleri L., et al.: Wave modelling – The state of the art, Progress in Oceanography, Vol. 75 (4), p 603-674, 2007

Collecte Localisation Satellites (CLS): Level-2P-Derived products from SWIM instrument of CFOSAT, CNES, https://doi.org/10.24400/527896/a01-2024.005, 2025

De Carlo M., Ardhuin F., Ollivier, A., Nigou A: Wave groups and small scale variability of wave heights observed by
610 altimeters, Journal of Geophysical Research, Oceans, 128 (8), e2023JC019740 doi:10.1029/2023JC019740, 2023

Elfouhaily, T. C., B. Chapron, K. Katsaros, and D. Vandemark: A unified directional spectrum for long and short wind-driven waves, J. Geophys. Res.,15,781-15,796, 1997

Forristall G.Z. and J.A. Greenwood: Directional spreading of measured and hindcasted wave spectra, Proceedings of the 5th International Workshop on Waves, Storm Surges and Coastal Hazards, available on line www.waveworkshop.org/ , 1998

Gagnaire-Renou, E., M. Benoit, and P. Forget: Ocean wave spectrum properties as derived from quasi-exact computations of nonlinear wave-wave interactions, J. Geophys. Res. Ocean, 115, C12058, doi:10.1029/2009JC005665, 2010

https://doi.org/10.5194/essd-2026-928
Preprint. Discussion started: 26 November 2026
© Author(s) 2026. CC BY 4.0 License.



Gemmrich, J., Cicon, L.: Generation mechanism and prediction of an observed extreme rogue wave, Sci Rep 12, 1718, https://doi.org/10.1038/s41598-022-05671-4, 2022

Giordani H., L.Aouf, and A. Dalphinet: Insights into Ocean Surface Wave Feedback on the Atmosphere in the Western Tropical Atlantic, In revision, Ocean Dynamics, 2026

Goda, Y.: Random seas and design of maritime structures, Advanced series on ocean engineering, Vol.33, Third edition, Edited by Word scientific Publishing Co, 2010, ISBN-13:978-981-4282-39-0, 2010

Häfner D., Gemmrich J., and Jochum M.: FOWD: A Free Ocean Wave Dataset for Data Mining and Machine Learning. Journal of Atmospheric and Oceanic Technology. 10.1175/JTECH-D-20-0185.1. , 2021

Hauser D., C. Tison, T. Amiot, L. Delaye, N. Corcoral et al.: SWIM: the first spaceborne wave scatterometer, IEEE Trans. on Geoscience and remote Sensing, 10.1109/TGRS.2017.2658672 , Vol. 55, 5, 2017

Hauser D., Tourain C., Hermozo L., Alraddawi D., Aouf L., et al.: New observations from the SWIM radar on board CFOSAT: instrument validation and ocean wave measurement assessment, IEEE Transactions on Geoscience and Remote Sensing, 59 (1), pp.5-26, doi: 10.1109/TGRS.2020.2994372, 2021

Janssen P.A.E.M. and J-R. Bidlot: On the extension of the freak wave warning system and its verification, ECMWF Technical Memorandum, 588, 2009

Kenyon, K.: Stokes Drift for Random Gravity Waves. J. Geophys. Res., 74(28), 6991-6994, 1969

Kuik, A. J., G. P. van Vledder, and L. H. Holthuijsen: A Method for the Routine Analysis of Pitch-and-Roll Buoy Wave Data. J. Phys. Oceanogr., 18, 1020–1034, https://doi.org/10.1175/1520-0485(1988)018<1020:AMFTRA>2.0.CO;2, 1988

Law Chune, S., Aouf, L.: Wave effects in global ocean modeling: parametrizations vs. forcing from a wave model, Ocean Dynamics 68, 1739–1758, https://doi.org/10.1007/s10236-018-1220-2, 2018

Leibovich S.: The form and dynamics of Langmuir circulations, Ann. Rev. Fluid Mech., 15:391-427 (1983), https://doi.org/10.1146/annurev.fl.15.010183.002135, 1983

Le Merle D., D. Hauser, C.Yang: Wave field properties in tropical cyclones from the spectral observation of the CFOSAT/SWIM spaceborne instrument, J. Geophys. Res., 128, e2022JC019074, 2022

Longuet-Higgins M. S.: On the joint distribution of wave periods and amplitudes in a random wave field, Proc. R . Soc. Lond. A 389, 241-258, 1983

Melet, A., Meyssignac, B., Almar, R. *et al.:* Under-estimated wave contribution to coastal sea-level rise. Nature Clim Change 8, 234–239, https://doi.org/10.1038/s41558-018-0088-y, 2018

Meucci A., Young Ian R., Pepler A., Rudeva I., Ribal A., Bidlot J.R, Babanin A.V.: Evaluation of Spectral Wave Models Physics as Applied to a 100-Year Southern Hemisphere Extra-Tropical Cyclone Sea State, Journal of Geophysical Research: Oceans, 128, e2023JC019751, 2023

Mori, N., Onorato, M., & Janssen, P. A. E. M.: On the estimation of the kurtosis in directional sea states for freak wave forecasting. Journal of Physical Oceanography, 41, 1484–1497, https://doi.org/10.1175/2011JPO4542.1, 2011

Phillips, O. M.: The equilibrium range in the spectrum of wind-generated waves. J. Fluid Mech., 426, 1958

https://doi.org/10.5194/essd-2026-928
Preprint. Discussion started: 26 November 2026
© Author(s) 2026. CC BY 4.0 License.



Pouplin, C., Mouche, A., and Chapron, B. : A multi-sensor approach for the characterization of tropical cyclone induced swell—Application to TC Larry, Geophysical Research Letters, 51,e2024GL109712, 2021

Rabault , J. Voermans, T. Nose, G. Sutherland, A. Babanin, et al: Observations of high-frequency spectral peaks from in-situ waves in ice data: evidence for nonlinear waves in ice triad interactions?, arXiv:2507.19034 [physics.geo-ph], https://doi.org/10.48550/arXiv.2507.19034, 2026

Rogers W. E., and G.P. Van Vledder: Frequency width in predictions of windsea spectra and the role of the nonlinear solver, Ocean Modelling 70, 52–61, 2013, doi 10.1016/j.ocemod.2012.11.010, 2013

Rogers W.E. and D. W. C. Wang: Directional validation of wave predictions, Journal of Atmospheric and Oceanic Technology, 24, 504-520, 10.1175/JTECH1990.1, 2007

Rosenthal, W., and Lehner, S., Rogue Waves: Results of the MaxWave Project." ASME. *J. Offshore Mech. Arct. Eng*., 130(2): 021006. https://doi.org/10.1115/1.2918126 , 2008

Serio L., M. Onorato, A. R. Osborne and P. A. E. M. Janssen: On the computation of the Benjamin-Feir Index, Il nuovo cimento, Vol. 28 C, N. 6, DOI 10.1393/ncc/i2005-10134-1, 2005

Socquet-Juglard H., Dysthe K., Trulsen K., Krogstad H., Liu J. Probability distributions of surface gravity waves during spectral changes. Journal of Fluid Mechanics, 542:195-216. doi:10.1017/S0022112005006312, 2005

Tourain C., *et al*.: CFOSAT: Products Reprocessing and Contributions in Oceanography, 2023 IEEE International Geoscience and Remote Sensing Symposium, Pasadena, CA, USA, pp. 3958-3961, doi: 10.1109/IGARSS52108.2023.10283105, 2023

Tayfun M.A., and Fedele F.: Wave-height distributions and nonlinear effects, Ocean Eng. 34 (11-12), 1631–1649. https://doi.org/10.1016/j.oceaneng.2006.11.006, 2007

Thorpe S.A.: Langmuir circulation, Annual Review of Fluid Mechanics 36:55-79, https://doi.org/10.1146/annurev.fluid.36.052203.071431, 2004

Voermans J., Rabault J., Filchuk K., Ryzhov I., Heil P., Marchenko A, Collins III C.O , Dabboor M., Sutherland G. , and Babanin A.V. : Experimental evidence for a universal threshold characterizing wave-induced sea ice break-up, The Cryosphere, 14, 4265–4278, https://doi.org/10.5194/tc-14-4265-2020, 2020

Wamdi Group: The WAM Model—A Third Generation Ocean Wave Prediction Model, Journal of Physical Oceanography, vol 18(12), p 1775–1810, doi: 10.1175/1520-0485(1988)018<1775:TWMTGO>2.0.CO;2, 1988

Wang He, Mouche A., Husson R, Chapron B., Jingsong Yang , Jianqiang Liu , and Lin Ren: Quantifying uncertainties in the partitioned swell heights observed from CFOSAT SWIM and Sentinel-1 SAR via Triple Collocation, IEEE Trans. On Geosc. and Remote Sens., Vol.60, pp. 1-16, doi:10.1109/TGRS.2022.3179511, 2022

Webb A., Fox-Kemper B.: Impacts of wave spreading and multidirectional waves on estimating Stokes drift, Ocean Modelling, Volume 96, Part 1, Pages 49-64, doi:10.1016/j.ocemod.2014.12.007, 2015

Xu Ying, Hauser D., Jianqiang Liu, Jianyang Si, Chen Yan, Shufen Chen, Junmin Meng, Chenqing Fan, Meijie Liu, Ping Chen: Statistical comparison of ocean wave directional spectra derived from SWIM/CFOSAT satellite observations and from buoy observations, IEEE Transactions on Geoscience and Remote Sensing,vol 60, p1-20, doi: 10.1109/TGRS.2022.3199393, 2022

https://doi.org/10.5194/essd-2026-928
Preprint. Discussion started: 26 November 2026
© Author(s) 2026. CC BY 4.0 License.



Young I.R: The determination of confidence limits associated with estimates of the spectral peak frequency, Ocean Engineering, Vol. 22, No. 7, pp. 669-686, 1995

Zhao Xiaolu, L. Oruba, D. Hauser, B. Zhang and E. Dormy: What can Hurricane Sam (2021) tell us about extreme ocean waves under tropical cyclones? Journal of Geophysical Research: Oceans, JGRC26037, doi: 10.1029/2024JC020957, 2024

Zieger S., A.V. Babanin ,W. E. Rogers and I. R. Young: Observation-based source terms in the third-generation wave model WAVEWATCH, Ocean Modelling , 96, 2-25, doi: 0.1016/j.ocemod.2015.07.014, 2015

Zou Shihao , D.Hauser, C.Peureux, Qing Li: Fusing SAR and SWIM Observations to Improve the Global Stokes Drift Estimates, in press, in Remote Sensing of Environment, 2026